ARTICLE NO. 77-68

A New Single-Rotation-Axis Autopilot for Rapid Spacecraft Attitude Maneuvers

L.A. D'Amario* and G.S. Stubbs*
The Charles Stark Draper Laboratory, Inc., Cambridge, Mass.

Rapid attitude maneuvers of a space vehicle are facilitated by a single-rotation-axis (SRA) digital autopilot that accurately compensates for nonlinear angular-velocity coupling effects to achieve nearly maximum jet-torquing capabilities. The SRA autopilot utilizes the principle that an attitude maneuver can be effected by rotating the vehicle about an axis fixed to the body and stationary in the inertial attitude reference frame. The autopilot is designed to produce regular closely spaced jet firings whose effects may be modeled in premaneuver computations by continuously varying forces and torques. The translational ΔV produced by attitude jets fired singly during a manuever are accurately predicted from expected attitude-response and jet-firing patterns. Simulations of attitude maneuvers as large as 180 deg with SRA rates up to 40 deg/s have resulted in terminal attitude and attitude-rate errors of less than 1.5 deg and 1.5 deg/s, respectively. Per-axis errors in predicted ΔV have typically been less than 5% of the total ΔV.

I. Introduction

ACCORDING to a theorem of Euler,[1] the attitude of a body can be changed from any given orientation to any other orientation by rotating the body about an axis that is fixed to the vehicle and stationary in inertial space. This theorem was applied to maneuvers of the Apollo spacecraft by Crisp and Keene,[2,3] who showed that for cases where the dynamics about three orthogonal jet control axes could be assumed to be decoupled, the propellant consumption of the attitude control jets could be minimized by rotation about this single maneuver-determined axis.

It will be shown in this paper that the single-rotation-axis (SRA) mode of maneuvering can also be conveniently implemented for the case where the control-axis dynamics are not decoupled – and where, in particular, there are significant "angular-velocity coupling effects," (corresponding to an appreciable magnitude of the crossproduct of the angular-velocity vector times the angular-momentum vector in the torque-momentum equation).†

The following analyses and simulation results show that it is possible, even with discrete-firing jets, to maneuver a space vehicle in a highly predictable manner about the SRA. This predictability results from the fixed geometrical relationships of the jets to the commanded rotation axis, and from the fixed proportionality of the angular rotations, angular rates, and angular accelerations about the three orthogonal body axes of the vehicle. These two properties make it possible to model precisely, via simple matrix equations, the effects of angular-velocity coupling, jet-torque coupling, and jet-torque limitations. They enable premaneuver computation of the commanded angular-acceleration vs time about the SRA that will utilize close to maximum jet-torquing capabilities to execute a maneuver within close tolerances in angular rate and angular rotation. These properties also make it possible to predict precisely the translational velocity changes that single firings of jets will produce in any given maneuver.

An SRA autopilot[6] will be described and analyzed which fires control jets intermittently throughout the SRA maneuver based on incrementally updated attitude errors and attitude rates for three orthogonal control (or "body") axes. Commands to this autopilot are issued in terms of incremental rotations and rates about the body axes. The feedback rates and body-angle increments will be assumed to be determined from measurements of the Advanced Inertial Reference System (AIRS).[7] This system is "gimbal-less," employing a floated ball at the stable member, and measuring attitude in terms of "band angles" determined by the intersections of three orthogonally mounted great-circle resolver bands on the ball with a single resolver band on the spherical case surrounding the ball.

II. Basic Relationships and Assumptions

Consider the general case of a rigid body rotating under the influence of body-mounted torquing devices. Let the applied torque vector τ, the angular velocity vector ω, and the inertia matrix I be expressed in terms of components along three orthogonal body axes represented by the unit vector triad B_1, B_2, B_3. Then, the rotational equation of motion may be written as

$$\tau = I\dot{\omega} + \Omega_\omega I\omega \tag{1}$$

where

$$\Omega_\omega = \begin{bmatrix} 0 & -\omega_3 & \omega_2 \\ \omega_3 & 0 & -\omega_1 \\ -\omega_2 & \omega_1 & 0 \end{bmatrix} \tag{2}$$

The three scalar equations represented by the vector expression of Eq. (1) take the general form

$$\tau_i = I_{ii}\dot{\omega}_i + I_{ij}\dot{\omega}_j + I_{ik}\dot{\omega}_k - (\omega_k^2 - \omega_j^2)I_{jk} + \omega_j\omega_k(I_{kk} - I_{jj}) - \omega_i(\omega_k I_{ij} - \omega_j I_{ik}) \tag{3}$$

Presented as Paper 77-68 at the AIAA 15th Aerospace Sciences Meeting Los Angeles, Calif., Jan. 24-26, 1977; submitted March 28, 1977; revision received Sept. 19, 1978.

Index categories: Spacecraft Dynamics and Control; Spacecraft Simulation.

*Staff Engineer, Control & Flight Dynamics Division. Member AIAA.

†The effects of angular-velocity coupling have also been considered by others for non-SRA maneuvers. For example, the use of short-duration jet impulses to initiate and terminate general attitude maneuvers has been studied by Dixon and others.[4,5]

where $(i,j,k) = (1,2,3), (2,3,1), (3,1,2)$. An inspection of Eq. (3) reveals that angular-velocity coupling arises from nonzero products of inertia and unequal moments of inertia.

Next, consider a general relationship between body-axis torques and control-jet firings

$$\tau = AS \tag{4}$$

The matrix A is called the jet-torque matrix, where $A = [a_{ij}]$, and a_{ij} is the torque about the ith body axis resulting from the firing of a jet or jets to produce torque about the jth body axis. The variable S is the jet-firing vector. Its roll, pitch, and yaw components take the values $+1$, 0, or -1 when the jet firing produces positive, zero, or negative torque, respectively, about the appropriate body axis. An implicit assumption here is that the jet configuration is such that there is one unique jet or set of jets that is fired to produce either positive or negative torque about each body axis. Therefore, each element of A can be at most double-valued

$$a_{ij} = \begin{cases} a_{ij}(+) & (S_j = 0,1) \\ a_{ij}(-) & (S_j = -1) \end{cases} \tag{5}$$

Note that either $a_{ij}(+)$ or $a_{ij}(-)$ may be used when $S_j = 0$.

The forces along the body axes resulting from jet firings that are not necessarily in the form of pure couples can be expressed similarly as

$$f = A'S \tag{6}$$

where the elements of the jet-force matrix A' are defined in a manner analogous to that for the jet-torque matrix.

Two basic assumptions that facilitate the implementation of the SRA autopilot and the prediction of maneuver-produced ΔV's are: the SRA autopilot causes the vehicle to rotate exactly about the SRA for the entire maneuver; and the effects of repetitive jet firings in a maneuver can be approximated by continuously varying forces and torques. (Note that the latter assumption is valid only if the autopilot produces nearly uniform jet-firing limit cycles whose periods are small relative to the length of time the vehicle is rotating.)

The first assumption allows the vehicle angular velocity to be expressed in terms of the single-axis rotation rate $\dot{\beta}$, and the unit rotation vector $\boldsymbol{r}$

$$\omega = \dot{\beta}\boldsymbol{r} \tag{7}$$

Under the assumption that the torque τ is continuously varied to maintain the body-fixed inertially fixed rotation axis $\boldsymbol{r}$, Eq. (7) may be used to simplify Eq. (1):

$$\tau = \boldsymbol{q}\ddot{\beta} - \boldsymbol{u}\dot{\beta}^2 \tag{8}$$

where $\boldsymbol{q} = I\boldsymbol{r}$, $\boldsymbol{u} = -\Omega_r \boldsymbol{q}$, and the definition of Ω_r is analogous to that of Ω_ω. The foregoing simplification of the torque expression from a dependence on the vector angular velocity ω and acceleration $\dot{\omega}$ to a dependence on the scalar single-axis rotation rate $\dot{\beta}$ and acceleration $\ddot{\beta}$ is an important feature of the SRA autopilot concept.

The second listed assumption allows Eqs. (4) and (6) to be rewritten to relate continuously varying limit-cycle-averaged values of τ and f to the fractional jet on-time vector $\boldsymbol{\delta}$

$$\tau = A\boldsymbol{\delta} \tag{9}$$

$$f = A'\boldsymbol{\delta} \tag{10}$$

where δ_j is a continuously varying quantity whose magnitude equals the fractional on-time of the jet or jets that control torque about the jth body axis, and whose sign denotes the polarity of the torque. Equation (5) now becomes

$$a_{ij} = \begin{cases} a_{ij}(+) & (\delta_j \geq 0) \\ a_{ij}(-) & (\delta_j < 0) \end{cases} \tag{11}$$

In computing command signals for the SRA autopilot, the fractional jet on-time $\boldsymbol{\delta}$ must be related to the single-axis rotation rate $\dot{\beta}$ and acceleration $\ddot{\beta}$. Combining Eqs. (8) and (9) yields

$$\boldsymbol{\delta} = \boldsymbol{g}\ddot{\beta} - \boldsymbol{h}\dot{\beta}^2 \tag{12}$$

where $\boldsymbol{g} = A^{-1}\boldsymbol{q}$ and $\boldsymbol{h} = A^{-1}\boldsymbol{u}$.

The prediction of maneuver ΔV's for the SRA autopilot requires that the time variation of the body-axis force components be expressed in terms of $\dot{\beta}$ and $\ddot{\beta}$. Combining Eqs. (10) and (12), one obtains

$$f = A'\boldsymbol{g}\ddot{\beta} - A'\boldsymbol{h}\dot{\beta}^2 \tag{13}$$

Here the components of A' must be updated in accordance with sign changes in $\boldsymbol{\delta}$ obtained from Eq. (12). The foregoing derivations have shown that τ, $\boldsymbol{\delta}$, and f may all be expressed in terms of $\ddot{\beta}$ and $\dot{\beta}^2$ for SRA maneuvers.

III. SRA Autopilot Premaneuver Computations

Single-Rotation Axis and Angle-to-Go

An SRA maneuver is defined in terms of two quantities. The first is the unit rotation vector $\boldsymbol{r}_0$, which denotes the axis of rotation required to perform an attitude change as a rotation about a single body-fixed inertially fixed axis. The second quantity is the initial angle-to-go α_0, the angle through which the vehicle must be rotated about $\boldsymbol{r}_0$ to achieve the desired attitude change. The SRA autopilot requires the premaneuver computation of $\boldsymbol{r}_0$ and α_0 as the first step in the calculation of maneuver commands and predicted ΔV.

Let it be assumed that in the case of an AIRS-based autopilot, the desired final body axes $\boldsymbol{B}_1''$, $\boldsymbol{B}_2''$, $\boldsymbol{B}_3''$ for the maneuver are defined relative to the AIRS platform axes, $\boldsymbol{P}_1$, $\boldsymbol{P}_2$, $\boldsymbol{P}_3$, by the platform-axes-to-final-body-axes transformation matrix $C_{b''}^{p}$. Then, using the Inertial Measurement Unit (IMU) measured transformation between the platform axes, and the initial body axes $\boldsymbol{B}_1'$, $\boldsymbol{B}_2'$, $\boldsymbol{B}_3'$, denoted as $C_{b'}^{p}$, the transformation between the initial and final body axes (attitudes) is computed from

$$C_{b''}^{b'} = C_{b''}^{p} C_{b'}^{p\,T} \tag{14}$$

The matrix $C_{b''}^{b'}$, which may be called the "initial error matrix," is employed to determine $\boldsymbol{r}_0$, α_0 values as follows, where $C_{b''}^{b'} = [C_{ij}]$

$$\alpha_0 = \cos^{-1}[\tfrac{1}{2}(C_{11} + C_{22} + C_{33} - 1)] \tag{15}$$

$$r_{0_1} = \frac{C_{23} - C_{32}}{2\sin\alpha_0} \tag{16}$$

$$r_{0_2} = \frac{C_{31} - C_{13}}{2\sin\alpha_0} \tag{17}$$

$$r_{0_3} = \frac{C_{12} - C_{21}}{2\sin\alpha_0} \tag{18}$$

Modifications of the preceding expressions are necessary when α_0 is close to 0 or 180 deg (see Ref. 8, p. 1-91).

Commanded SRA Acceleration

An attitude maneuver, as performed by the SRA autopilot presented here, contains an acceleration period at the

beginning of the maneuver and a deceleration period toward the end. There may also be an intermediate coasting period with a constant rotation rate depending on the magnitude of the maneuver and limitations, if any, on maximum rotation rates.

There are two rotation angles used in describing an SRA maneuver. One is the previously mentioned angle-to-go, α, defined here as the angle through which the vehicle must rotate to go from any attitude in the maneuver to the desired final attitude. This angle has an initial value α_0 computed prior to the maneuver, and ideally should be reduced to zero at the end of the maneuver at which time $\dot{\alpha}$ should also be zero. The other rotation angle is β, the angle through which the vehicle has rotated from the initial attitude at any time in the maneuver. This angle is initially zero and should become equal to α_0 at the end of the maneuver, at which time $\dot{\beta}$ should be zero. The angles β and α are related by $\beta=\alpha_0-\alpha$; therefore $\dot{\beta}=-\dot{\alpha}$ and $\ddot{\beta}=-\ddot{\alpha}$. Maneuver commands are expressed in terms of $\ddot{\beta}$, $\dot{\beta}$, and β.

The fractional jet on-time for any channel (roll, pitch, or yaw) is given by Eq. (12). For a general unconstrained maneuver, in order to make most efficient use of the available jet torques, the value of commanded $\ddot{\beta}$ must be adjusted during the manuever so that the fractional jet-on-time of at least one channel always has nearly unity magnitude. Analytically this requirement means that at any point during the acceleration and deceleration periods of the maneuver, the commanded $\ddot{\beta}$ is the minimum, in magnitude, of three possibilities found by solving Eq. (12) for $\ddot{\beta}$, with the added condition that $|\delta_i|=\gamma$, wher γ is close to unity

$$\ddot{\beta}_i=(I/g_i)\,[\gamma\,\sin(\delta_i)+\dot{\beta}^2 h_i] \tag{19}$$

(The subscript i is added to $\ddot{\beta}$ to denote the fact that there are three possible values of $\ddot{\beta}$ corresponding to $|\delta_i|=\gamma$, $i=1,2,3$.)

The factor γ, which is called the "angular acceleration reduction factor," insures that the commanded acceleration is slightly less than the acceleration capability and corresponds to a fractional jet on-time for the limiting channel which is slightly less than unity (i.e., equal to γ). The reduction in commanded acceleration provides a safety margin for errors in the approximations used in computing the maximum available acceleration, and allows the jets to have a slight excess in acceleration capability to compensate for the lag in the autopilot's initial response to acceleration and deceleration commands. This lag is caused by the attitude error deadzone in the autopilot, whose structure is discussed in the next section.

The curves of $\ddot{\beta}_i$ vs $\dot{\beta}^2$ for $|\delta_i|=\gamma$ are straight lines which may intersect. Depending on the signs of g_i and h_i, the effect of angular-velocity coupling may either increase or decrease the acceleration capability of any channel during the acceleration period; but it must necessarily have the opposite effect during deceleration.

In addition to utilizing nearly maximum acceleration capabilities of at least one channel at all times, the time history of commanded $\ddot{\beta}$ must insure that certain boundary conditions are satisfied. Given that $\dot{\beta}=0$ and $\beta=0$ at $t=0$, the time at which the maneuver begins, the final conditions $\dot{\beta}=0$ and $\beta=\alpha_0$ at $t=T_f$, the time at which the maneuver ends, must be achieved. The end-of-maneuver time T_f must also be determined in the premaneuver computations.

An analytical determination of commanded $\ddot{\beta}$ vs time was rejected due to difficulties presented by the nonlinearity of the governing differential equation, the split-time boundary conditions, and the limiting channel switching. To overcome these difficulties, a simple procedure for computing premaneuver commands has been developed that involves approximating $\ddot{\beta}$ vs time by a staircase function. The procedure starts with the computation of $\ddot{\beta}$ at both ends of the maneuver and works toward the middle in a stepwise manner. At the lth step in the procedure, levels of acceleration and deceleration ($\ddot{\beta}_{l_{acc}}$, $\ddot{\beta}_{l_{dec}}$) are calculated from Eq. (19) so as to maximize the fractional jet on-time of at least one channel. Then the intervals of time ($\Delta T_{l_{acc}}$, $\Delta T_{l_{dec}}$) are computed from the requirement that during these intervals the angular rate $\dot{\beta}$ must increase by a specific step size $\Delta\dot{\beta}$, which remains constant for each step.

At each step, once the limiting value of $\ddot{\beta}$ is determined, Eq. (12) is used to compute $\boldsymbol{\delta}$ so that the A matrix can be updated and new $\boldsymbol{g}$ and $\boldsymbol{h}$ values computed if the fractional jet on-time of a nonlimiting channel changes sign. The component of $\boldsymbol{\delta}$ corresponding to the limiting channel is constrained by the method to have close to unit magnitude at the beginning of each acceleration step and at the end of each deceleration step.

The procedure is halted either when the accumulated $\dot{\beta}$ reaches a prespecified maximum allowable value $\dot{\beta}_{max.}$ or when the accumulated rotation angle β reaches α_0, the initial angle-to-go for the maneuver. In the former case, the maneuver is said to be "saturated," and the length of the period during which $\dot{\beta}$ is constant is calculated to achieve a total rotation equal to α_0. This period will henceforth be referred to as the "coasting" period, although in general an applied torque is required to maintain $\dot{\beta}$ constant. In the latter case, the maneuver is "unsaturated," and there is no coasting period.

When the step-by-step computation procedure is completed, the information that has been generated consists of a set of levels of acceleration and deceleration ($\ddot{\beta}_{l_{acc}}$ and $\ddot{\beta}_{l_{dec}}$), the time intervals of application of these accelerations ($\Delta T_{l_{acc}}$ and $\Delta T_{l_{dec}}$) and the duration of the coasting period (ΔT_{coast}), if one is necessary. From this information, a staircase time history of commanded $\ddot{\beta}$ can be constructed in terms of vectors of acceleration levels and switching times.

ΔV Prediction

It can be shown (see Ref. 8, pp. A-6, A-7) that if f is defined as the force, in current body axes, resulting from jet firings at any point in the maneuver, then the total maneuver-produced velocity increment ΔV referred to the initial body axes, B_1', B_2', B_3' is given by

$$\Delta V=\frac{1}{M}\left\{[\Omega_r\Omega_r+J]\int_0^{T_f} f\,dt-\Omega_r\Omega_r\int_0^{T_f} f\cos\beta\,dt+\Omega_r\int_0^{T_f} f\sin\beta\,dt\right\} \tag{20}$$

where Ω_r is as defined in Sec. II, J is the identity matrix, T_f is the computed end-of-maneuver time, and M is the vehicle mass.

The SRA autopilot's ΔV prediction computations are carried out in terms of three vectors that are summed to obtain ΔV

$$\Delta V=\Delta V_{acc}+\Delta V_{coast}+\Delta V_{dec} \tag{21}$$

The first and last components are obtained by approximate numerical integration of Eq. (20) in the acceleration and deceleration periods, assuming that the force vector in each constant-$\ddot{\beta}$ region is constant and equal to the mean of the two force vectors computed for the beginning and end of each constant-$\ddot{\beta}$ interval.

The second component of Eq. (21) is obtained by analytical integration of the effects of the constant vector $f=\bar{f}_{coast}$ resulting from the substitution into Eq. (10) of the constant vector $\boldsymbol{\delta}=\boldsymbol{\delta}_{coast}$, which is obtained from

$$\boldsymbol{\delta}_{coast}=-\boldsymbol{h}\dot{\beta}^2_{coast} \tag{22}$$

where $\dot{\beta}_{coast}$ is the constant value of $\dot{\beta}$ in the coast region.

Expressions for the three vector components compressing ΔV are as follows:

$$\Delta V_{\text{acc}} = \sum_{l=1}^{m} \left(\frac{\Delta T_{l_{\text{acc}}}}{M}\right) C_{b'}^{\tilde{b}}\Big|_{\tilde{\beta}=\tilde{\beta}_{l_{\text{acc}}}} \tilde{f}_{l_{\text{acc}}} \tag{23a}$$

$$\Delta V_{\text{dec}} = \sum_{l=1}^{m} \left(\frac{\Delta T_{l_{\text{dec}}}}{M}\right) C_{b'}^{\tilde{b}}\Big|_{\tilde{\beta}=\tilde{\beta}_{l_{\text{dec}}}} \tilde{f}_{l_{\text{dec}}} \tag{23b}$$

$$\Delta V_{\text{coast}} = \left(\frac{\Delta T_{\text{coast}}}{M}\right)\left[J + \left(1 - \frac{\sin(\Delta\beta_{\text{coast}}/2)}{(\Delta\beta_{\text{coast}}/2)}\cos\tilde{\beta}_{\text{coast}}\right)\Omega_r\Omega_r + \frac{\sin(\Delta\beta_{\text{coast}}/2)}{(\Delta\beta_{\text{coast}}/2)}\sin\tilde{\beta}_{\text{coast}}\Omega_r\right]\tilde{f}_{\text{coast}} \tag{24}$$

where

$$C_{b'}^{\tilde{b}} = \Omega_r\Omega_r(1-\cos\tilde{\beta}) + \Omega_r\sin\tilde{\beta} + J \tag{25}$$

Other new symbols used in Eqs. (23) and (24) are defined as follows:

l	= integer denoting a particular step in the acceleration or deceleration period
m	= the total number of pairs of acceleration and deceleration steps in the maneuver
$\tilde{\beta}_{l_{\text{acc}}}, \tilde{\beta}_{l_{\text{dec}}}$	= mean values of the initial and final β in the acceleration time interval $\Delta T_{l_{\text{acc}}}$ and deceleration time interval $\Delta T_{l_{\text{dec}}}$, respectively
$\tilde{\beta}_{\text{coast}}$	= value of β in the middle of the "coasting period"
$\Delta\beta_{\text{coast}}$	= change in β which occurs over the "coasting period"

The quantities $\tilde{f}_{l_{\text{acc}}}$ and $\tilde{f}_{l_{\text{dec}}}$ are defined similarly to $\tilde{\beta}_{l_{\text{acc}}}$ and $\tilde{\beta}_{l_{\text{dec}}}$.

IV. SRA Autopilot Maneuver Computations

SRA Autopilot Structure

An SRA attitude maneuver is implemented by commanding an intermediate attitude that coincides with the initial attitude at $t=0$ and with the final desired attitude at $t=T_f$. The commanded attitude during the maneuver is the attitude achieved by rotating the vehicle about $\boldsymbol{r}_0$ through an angle β where β is the commanded single-axis rotation angle, obtained as the double integration of the staircase time history of commanded $\ddot{\beta}$.

The structure of the SRA-maneuver autopilot is illustrated in Fig. 1. The autopilot attitude error vector $\boldsymbol{E}$ is computed from the following simple incremental relationship:

$$\boldsymbol{E}_n = \boldsymbol{E}_{n-1} + \Delta\boldsymbol{\theta}_{c_n} - \Delta\boldsymbol{\theta}_n$$

where $\Delta\boldsymbol{\theta}_{c_n}$ and $\Delta\boldsymbol{\theta}_n$ are vectors containing small incremental rotations about the current body axes, which are commanded and measured, respectively, at every autopilot sampling time, $t=nT$, where $T=0.03$ s.

These increments are determined as follows. The commanded body-angle increment is computed from

$$\Delta\theta_{c_n} = (\beta_n - \beta_{n-1})r_0$$

where β_n and β_{n-1} are values of commanded β at successive autopilot sampling instants, based on the $\ddot{\beta}$ time history. The measured body-angle increment is calculated from an equation that relates $\Delta\theta_n$ to increments in the AIRS Inertial Measurement Unit (IMU) band angles over each sampling interval. This calculation is described later in this section.

Referring again to Fig. 1, the attitude error $\boldsymbol{E}$ is scaled and then added to the rate error, computed as the difference between the commanded and estimated body rates, in order to generate the input to the deadzone logic that determines jet-firing commands $\boldsymbol{S}$. The commanded rate is calculated as

$$\omega_{c_n} = \dot{\beta}_n r_0$$

and the estimated rate is updated based on body-angle-increment data, jet-firing commands, and the commanded single-axis rotation rate. The computation of the rate estimate is described later in this section.

The jet-section logic chooses the jet or combination of jets that produces positive or negative torque about a body axis if the jet-firing command vector is $+1$ or -1, respectively. It has been assumed that there is one unique jet or combination of jets that produces positive or negative torque about any body axis.

Attitude Error Reinitialization

At the end of the maneuver (that is, when the commanded attitude reaches the desired final attitude at $t=T_f$), the SRA autopilot is switched to an attitude-hold mode in which autopilot commands are zeroed, i.e., $\Delta\boldsymbol{\theta}_c$ and $\boldsymbol{\omega}_c$ are set equal to zero. Also at that time, the attitude error vector $\boldsymbol{E}$ is reinitialized by setting $\boldsymbol{E}$ equal to the product $\alpha\boldsymbol{r}$ where $\boldsymbol{r}$ and α correspond to the small SRA maneuver from the measured end-of-maneuver attitude to the desired final attitude. These two attitudes should be nearly equal if the vehicle followed the autopilot commands accurately.

Attitude Processing

The attitude of AIRS is measured by means of printed-circuit resolver bands that are mounted on the outer surface of the floated ball and on the inner surface of the spherical shell (or "case") that surrounds the ball. Three orthogonal great-circle "driver" bands are mounted on the ball, and one great-circle "receiver" band is mounted on the inside of the spherical shell. Each driver band intersects the receiver band at two points, one of which is selected by the IMU electronics

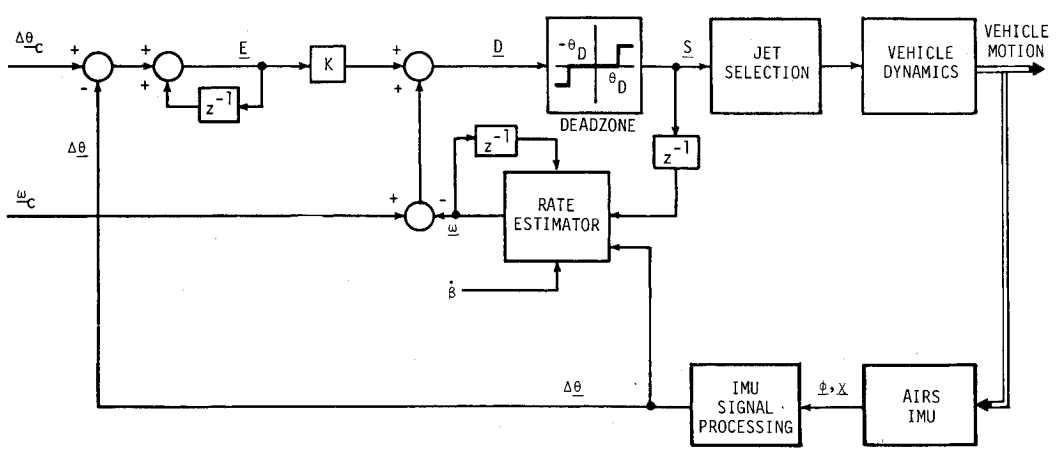

Fig. 1 SRA maneuver autopilot block diagram.

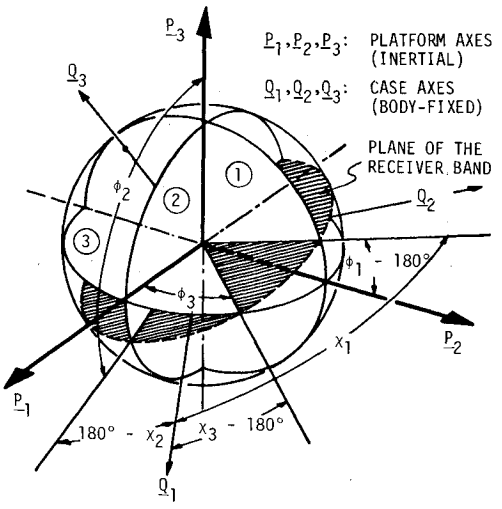

Fig. 2 Definition of the AIRS band angles.

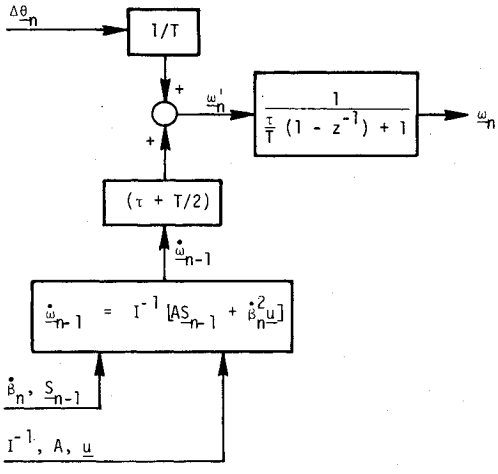

Fig. 3 Rate estimator.

for attitude definition. The IMU electronics measure the location of the selected intersection point of any band pair in terms of the angular position of that point along each band from a reference point on the band. These band angles, which are shown in Fig. 2, are defined as ϕ_1, ϕ_2, ϕ_3 for the three driver bands, and as χ_1, χ_2, χ_3 for the receiver band. Thus, the intersection of the jth driver band with the receiver band is measured by the angles ϕ_j and χ_j along these bands.

IMU attitude data are processed by the SRA autopilot in order to compute the transformation matrix C_b^p which relates the body axes triad $\boldsymbol{B}_1$, $\boldsymbol{B}_2$, $\boldsymbol{B}_3$ to the IMU platform axis triad $\boldsymbol{P}_1$, $\boldsymbol{P}_2$, $\boldsymbol{P}_3$, and the body-angle-increment vector $\Delta\theta_n$ whose components are the incremental rotations of the vehicle about the roll, pitch, and yaw axes as measured by the IMU over the time interval $t=(n-1)\,T$ to $t=nT$.

The body-angle increments are computed from the AIRS band-angle increments every autopilot cycle for use in generation of autopilot attitude errors. The matrix C_b^p, on the other hand, is computed only at the beginning and end of the maneuver to enable the determination of r, α values at those times in the former case for the calculation of maneuver commands, and in the latter case for the reinitialization of attitude error for the postmaneuver attitude hold mode. Since only two pairs of band angles are needed for determining the ball case orientation, AIRS signal processing computations reject the least accurate pair of band angles, which is the pair associated with the driver band that is most nearly parallel to the receiver band.

General relationships for the elements of a platform-axes-to-body-axes transformation matrix C_b^p, and for the elements of a band-angle-increment-to-body-angle-increment matrix B may be derived[9-11] in terms of cyclic subscripts $(i, j, k) = (1, 2, 3,), (3, 2, 1), (2, 1, 3)$, where k is the number of the rejected band. Since the SRA autopilot uses incremental feedback based on the B matrix, except at the beginning and end of the maneuver, the form of this matrix is of prime interest. The B matrix is used to compute elements of the body-angle increment vector $\Delta\theta_n$ from the band-angle-increment vector $\Delta\psi_n$ for the nth autopilot cycle, according to $\Delta\theta_n = B_n\Delta\psi_n$, where $\Delta\psi_n = [\Delta\phi_i, \Delta\phi_j, \Delta\chi_i]^T$. Here, it is assumed arbitrarily that the (body-fixed) case unit vectors $\boldsymbol{Q}_1$, $\boldsymbol{Q}_2$, $\boldsymbol{Q}_3$ defined in Fig. 2 are related to the unit body-axis vectors $\boldsymbol{B}_1$, $\boldsymbol{B}_2$, $\boldsymbol{B}_3$ by the relationships $\boldsymbol{Q}_1 = \boldsymbol{B}_3$, $\boldsymbol{Q}_2 = -\boldsymbol{B}_2$, and $\boldsymbol{Q}_3 = \boldsymbol{B}_1$. The elements of the matrix B are given by

$$B_{11} = -w\cos\phi_i\cos\phi_j \qquad B_{12} = 0 \qquad B_{13} = -1$$

$$B_{21} = w^2\sin\phi_j\sin\chi_j \qquad B_{22} = w^2\cos\phi_i\sin\chi_i$$

$$B_{23} = 0 \qquad B_{31} = -w^2\sin\phi_j\cos\chi_j$$

$$B_{32} = w^2\cos\phi_i\cos\chi_i \qquad B_{33} = 0$$

where $w = 1/[\sin(\chi_i - \chi_j)]$.

Although the band-angle increments and corresponding body-angle increments need to be computed every autopilot cycle, such is not the case for the B matrix. Autopilot responses and ΔV prediction accuracy are essentially unaffected if the B matrix is updated every 15 autopilot cycles (0.45 s) as long as the values of band angles used to update B are predictions of midpoint values in the next 0.45-s interval. The prediction is simply the current value of the band angle plus one half the increment over the last 0.45-s interval. The result of this simplification is a significant reduction in computation time and minimal degradation in autopilot performance.

Rate Estimator

The presence of deterministic errors and noise in the AIRS band-angle measurements makes it necessary to employ low-pass filtering in a rate estimator to minimize the adverse effects of these error sources. The undesirable time lag which would be introduced by a low-pass filter operating on band-angle measurements is effectively canceled out by the introduction into the rate estimator of an estimated angular acceleration about each body axis based on the maneuver geometry, the estimated mass properties, the estimated jet-torque coefficients and the known jet-firing commands for each autopilot sampling interval. The mechanization of this rate estimation scheme is shown in Fig. 3.

V. Simulation Results

A six-degree-of-freedom engineering simulation was written to test the SRA autopilot concepts presented in this paper. This simulation contains a driver program and subroutines for premaneuver command computations, premaneuver ΔV prediction computations, the digital autopilot, a vehicle model, an AIRS IMU model, and generation of plots.

Vehicle Model

The vehicle is modeled as a rigid body with constant mass properties. The differential equation describing the rotational dynamics of the vehicle is given by Eq. (1). Jet-firing commands in conjunction with precomputed jet torques yield the applied torque in each autopilot cycle, and the differential equation is integrated via a Runge-Kutta scheme. The ΔV produced by jet firings on each autopilot cycle is transformed to the initial body axes and accumulated for comparison with the predicted ΔV.

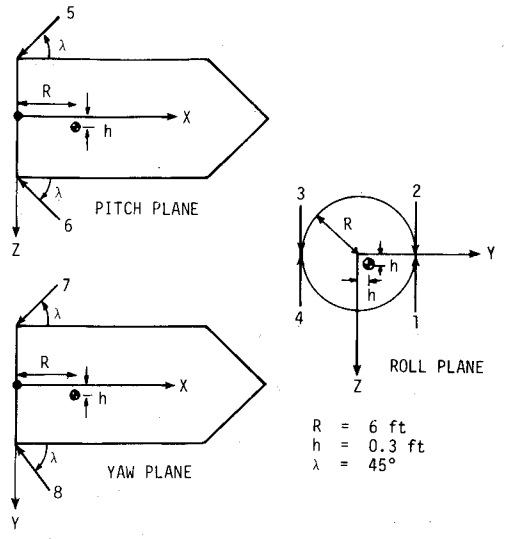

Fig. 4 Jet configuration.

IMU Model

In the simulation of the AIRS IMU, the true values of the band angles are propagated during the maneuver from their initial values. To these true values are added deterministic errors and noise, and then the result is quantized to obtain the measured band angles. The measured band angles are utilized in the attitude processing computations to generate measured body-angle increments, $\Delta\theta$, and the measured platform-to-body transformation matrix, C_b^g, as described in Sec. IV. The true C_b^g is used in the simulation for the aforementioned transformation of ΔV components to the initial body axes and for computation of true angles-to-go about each body axis for plotting purposes.

Illustrative Example

For this example, a hypothetical vehicle configuration, shown in Fig. 4, was chosen to provide significant amounts of angular-velocity coupling, torque coupling, and maneuver-produced ΔV in order to test the SRA autopilot concepts that account for these effects. The vehicle mass is 242 slugs, and its inertia matrix I in slug-ft^2 is

$$I = \begin{bmatrix} 874 & -316 & 287 \\ -316 & 4092 & -42.3 \\ 287 & -42.3 & 4494 \end{bmatrix}$$

The 50-lb pitch and yaw control jets and the 15-lb roll jets are located at the aft end of the vehicle. The pitch and yaw jets are fired singly, but the roll jets are fired as couples. The pitch and yaw acceleration capability is about 6 deg/s^2, and the roll acceleration capability is slightly more than twice that value.

The jet select logic is given in Table 1.

A simulation of a maneuver of the described vehicle with commanded rotations of 90 deg about the roll, pitch, and yaw axes was performed. For this maneuver, $\alpha_0 = 155.9$ deg and $r_0 = (0.577, 0.577, 0.577)$. The values of the simulation parameters are given in Table 2.

The mass-properties uncertainty factor is used to represent uncertainties in the knowledge of the vehicle mass properties that are used in the rate estimator to compute angular acceleration. The computer angular acceleration is multiplied by μ before being used in the estimated rate computation.

The results of the simulation are shown in Figs. 5 through 10. Figure 5 shows the time history of commanded SRA acceleration and rate during the maneuver. Note that $\ddot{\beta}$ decreases during the acceleration period; the limiting channel during acceleration is yaw. On the other hand, the magnitude of $\ddot{\beta}$ during deceleration increases initially but then decreases on the last two steps. The reason is that the limiting channel during deceleration switches from pitch to yaw. This maneuver is saturated and includes a coasting period such that the area under the $\dot{\beta}$-vs-time curve equals α_0.

Table 1 Jet selection logic

Jet firing command (S)	Control action	Selected jets
1, 0, 0	+Roll	2,4
−1, 0, 0	−Roll	1,3
0, 1, 0	+Pitch	5
0, −1, 0	−Pitch	6
0, 0, 1	+Yaw	8
0, 0, −1	−Yaw	7

Table 2 Values of simulation parameters

Maximum allowable SRA rate ($\ddot{\beta}_{\max.}$)	24 deg
Autopilot error gain (K)	1.0
Autopilot cycle time (T)	0.03 s
Rate-estimator time constant (τ)	0.5 s
Autopilot deadzone (θ_D)	0.8 deg
Mass-properties uncertainty factor (μ)	0.8
Angular-acceleration reduction factor (γ)	0.8
Autopilot command step size ($\Delta\dot{\beta}$)	4 deg/s
AIRS band-angle quantization	20 arc-s
AIRS driver band noise (1σ value)	60 arc-s
AIRS receiver band noise (1σ value)	20 arc-s

Table 3 Actual vs predicted ΔV

	X	Y	Z
Actual ΔV, fps	−1.0583	−1.7692	0.2115
Predicted ΔV, fps	−1.0264	−1.7090	0.2245

The true angles-to-go about the roll, pitch, and yaw axes during the maneuver are plotted in Fig. 6. All three curves begin at 90 deg and approach zero at the end of the maneuver in a well-behaved manner. There is negligible overshoot or undershoot with respect to the desired final attitude. The attitude-hold mode, which is initiated at the end of the maneuver, maintains the attitude of the vehicle very close to the desired final attitude.

The time histories of the measured body-angle increments and estimated body rates are displayed in Figs. 7 and 8, respectively. The erratic behavior of the body-angle increments is caused by the deterministic and noise components of the band-angle errors. Note how the estimated body rates have been smoothed by filtering in the rate estimator. Comparing Figs. 5 and 8, one can see that the autopilot rate response followed the commands closely.

Figure 9 shows the time histories of the incrementally updated autopilot attitude errors. The step changes at 10 s are caused by the reinitialization of the attitude errors at the beginning of the attitude-hold mode that follows the maneuver. The magnitudes of these step changes are very small, less than about 1.5 deg, which indicates that the simple incremental method of updating attitude errors yields a good measure of the actual attitude error throughout the maneuver.

The attitude errors are reinitialized to the measured angles-to-go at the end of the maneuver, and these values are a direct measure of the error between the final desired attitude and the actual end-of-maneuver attitude. For this maneuver, which had a total commanded rotation of 155.9 deg, the final attitude errors about the roll, pitch, and yaw axes are only −1.4, 0.8, and −0.9 deg respectively.

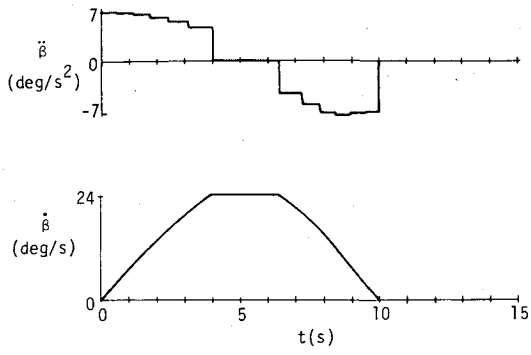

Fig. 5 Commanded SRA acceleration and rate.

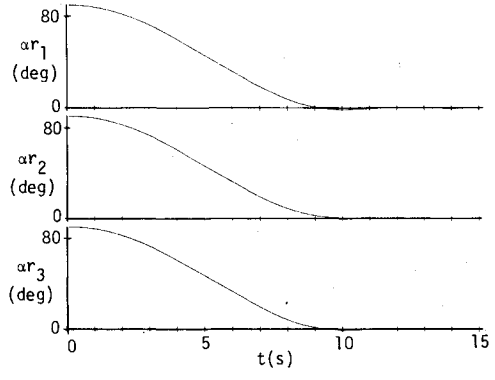

Fig. 6 Angles-to-go about the roll, pitch, and yaw axes.

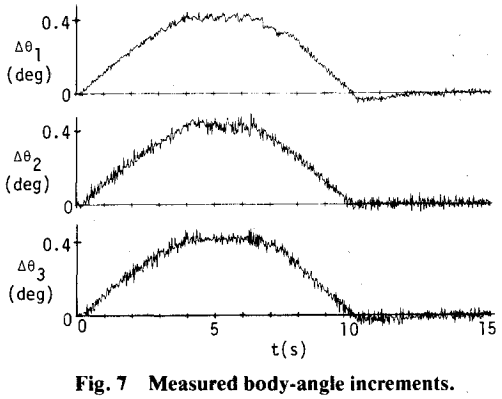

Fig. 7 Measured body-angle increments.

Figure 10 displays the time histories of the jet-firing commands. The periods of acceleration, coast, deceleration, and attitude-hold are also shown on this figure. It is evident from the jet-firing patterns that the yaw channel is the limiting channel during the acceleration period, and that first the pitch and then the yaw channel is the limiting channel during the deceleration period.

During the coast period, there is a significant amount of jet-firing activity, because even though the vehicle is not being commanded to accelerate, the jets must still fire to cancel the angular-velocity coupling effects. These effects, which are significant at these high rotation rates, would accelerate the vehicle in the absence of counteracting jet firings. During the coasting period, however, on-times are constant.

The jet-firing patterns show that there is little activity during the attitude-hold mode. This behavior indicates that the final attitude errors were small relative to the size of the autopilot deadzone. Finally, note that there is a time lag at the start of the maneuver before any jet firings occur. This time lag, which is also evident on Figs. 6 and 7, occurs because a finite amount of time passes at the start of the maneuver before the deadzone in the autopilot is exceeded.

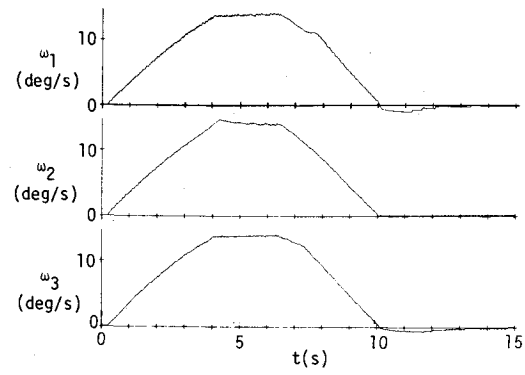

Fig. 8 Estimated body rates.

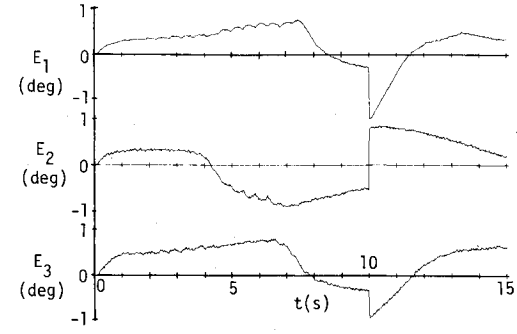

Fig. 9 Autopilot attitude errors.

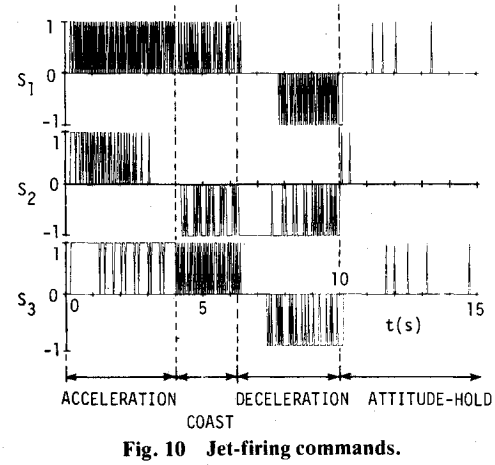

Fig. 10 Jet-firing commands.

The actual ΔV produced by maneuver jet firings during this simulated maneuver and the predicted ΔV determined as part of the premaneuver computations are given in Table 3, referred to the initial body axis. The error in the predicted ΔV is 3.4% of the resultant ΔV magnitude, and the largest per-axis error is 0.06 fps. For this maneuver, the ΔV caused by maneuver jet firings is accurately predictable.

VI. Conclusions

It has been demonstrated that the SRA autopilot concept developed in this paper, in conjunction with the all-attitude capability of AIRS, makes possible rapid unrestricted attitude maneuvers by taking into account accurately the effects of angular-velocity coupling and jet-torque coupling. In addition, the translational velocity changes produced during maneuvers by single firings of jets may be predicted accurately prior to the maneuver.

More specifically, the method of computing maneuver commands, which approximates the true continuously varying SRA acceleration capability by a stepwise time history, results in the accurate execution of maneuvers which utilize nearly maximum jet-torquing capabilities, and whose motion is highly predictable. The predictability of angular motion during the maneuver and the uniformity of jet-firing limit cycles, whose periods are small relative to the acceleration and deceleration periods, allow accurate predictions of maneuver-produced ΔV.

The incremental method of updating autopilot attitude errors during the maneuver has been shown to yield maneuver performance as good as that obtainable with an error-matrix approach while offering a substantial reduction in computation time. Finally, the SRA autopilot rate estimator, which processes band-angle increments to obtain body-axis rates, has demonstrated the ability to filter the significant deterministic errors and noise in the band-angle measurements to prevent spurious jet firings and to produce accurate body-axis rate information.

Acknowledgments

This research was performed at The Charles Stark Draper Laboratory, Inc. under Contract F04701-74-C-0047 with the Space and Missile System Organization of the Air Force Systems Command. Publication of this paper does not constitute approval by the U.S. Air Force of the findings or conclusions contained herein. It is published for the exchange and stimulation of ideas.

References

[1]Goldstein, H., *Classical Mechanics,* Addison-Wesley Publishing Co., Waltham, Mass., 1959, pp. 118-124, 132.

[2]Crisp, R. and Keene, D., "Attitude Maneuver Optimation to Conserve Reaction Control Propellants," Charles Stark Draper Laboratory, Cambridge, Mass., Rept. E-1832, Aug. 1965.

[3]Crisp, R. and Keene, D., "Apollo Command and Service Module Reaction Control by the Digital Autopilot," Charles Stark Draper Laboratory, Cambridge, Mass., Rept. E-1964, May 1966.

[4]Dixon, M.V., Edelbaum, T.N. Potter, J.E., and Vandevelde, W.E., "Fuel Optimal Reorientation of Axisymmetric Spacecraft," *Journal of Spacecraft and Rockets,* Vol. 7, Nov. 1970, pp. 1345-1351.

[5]Martz, C.W., "Attitude Reorientation of Spacecraft by Means of Impulse Coning," NASA TND-8452, Aug. 1977.

[6]D'Amario, L.A., and Stubbs, G.S., "A Single-Rotation-Axis Digital Autopilot Design which Compensates for Nonlinear Rotational Dynamics in Rapid Attitude Maneuvers of a Space Vehicle," Charles Stark Draper Laboratory, Cambridge, Mass., Rept. P-377, Dec. 1976.

[7]Miller, B., "MX Guidance Elements in Development, *"Aviation Week and Space Technology,* Vol. 105, Dec. 13, 1976, pp. 69-77.

[8]D'Amario, L.A., et al., "Final Report, Fiscal Year 1974–Advanced Targeting and Software Design Studies," Charles Stark Draper Laboratory, Cambridge, Mass., Rept. R-838, Aug. 1974.

[9]Rhodes, J.S., "Body Angular Rates in Terms of Measured Attitude Angles," Charles Stark Draper Laboratory, Cambridge, Mass., Memo No. 71-153 (revised), Oct. 4, 1971.

[10]Strunce, R., "Generalized Attitude Direction Cosine Matrix," Charles Stark Draper Laboratory, Cambridge, Mass., Memo No. 70-193, Dec. 9, 1970.

[11]Bleistein, N., "Transformation Matrix Computations for Attitude Readout System Incorporating Printed Pattern Receiver Band," Charles Stark Draper Laboratory, Cambridge, Mass., Memo No. 68-196, Dec. 8, 1968.